Metamaterial architecture from a self-shaping carnivorous plant

Caterina A. M. La Porta[a,b,1], Maria Chiara Lionetti[a,b], Silvia Bonfanti[a,c], Simone Milan[a,b], Cinzia Ferrario[a,b,d], Daniel Rayneau-Kirkhope[e], Mario Beretta[f], Maryam Hanifpour[e], Umberto Fascio[g], Miriam Ascagni[h], Larissa De Paola[c], Zoe Budrikis[a], Mario Schiavoni[i], Ermelinda Falletta[i], Alessandro Caselli[i], Oleksandr Chepizhko[j], Ausonio Tuissi[k], Alberto Vailati[c], and Stefano Zapperi[a,c,l,1]

[a]Center for Complexity and Biosystems, University of Milan, 20133 Milan, Italy; [b]Department of Environmental Science and Policy, University of Milan, 20133 Milan, Italy; [c]Department of Physics, University of Milan, 20133 Milan, Italy; [d]Department of Biology and Biotechnology "L. Spallanzani," University of Pavia, 27100 Pavia, Italy; [e]Department of Applied Physics, Aalto University, FI-00076 Aalto, Finland; [f]"Cittá Studi" Botanical Garden, Department of Biosciences, University of Milan, 20133 Milan, Italy; [g]Department of Biosciences, University of Milan, 20133 Milan, Italy; [h]UNITECH NOLIMITS, University of Milan, 20133 Milan, Italy; [i]Department of Chemistry, University of Milan, 20133 Milan, Italy; [j]Institut für Theoretische Physik, Leopold Franzens Universität Innsbruck, A-6020 Innsbruck, Austria; [k]Consiglio Nazionale delle Ricerche, Istituto di Chimica della Materia Condensata e di Tecnologie per l'Energia, 23900 Lecco, Italy; and [l]Consiglio Nazionale delle Ricerche, Istituto di Chimica della Materia Condensata e di Tecnologie per l'Energia, 20125 Milan, Italy

Edited by Tom C. Lubensky, University of Pennsylvania, Philadelphia, PA, and approved August 1, 2019 (received for review March 22, 2019)

As meticulously observed and recorded by Darwin, the leaves of the carnivorous plant *Drosera capensis* L. slowly fold around insects trapped on their sticky surface in order to ensure their digestion. While the biochemical signaling driving leaf closure has been associated with plant growth hormones, how mechanical forces actuate the process is still unknown. Here, we combine experimental tests of leaf mechanics with quantitative measurements of the leaf microstructure and biochemistry to demonstrate that the closure mechanism is programmed into the cellular architecture of *D. capensis* leaves, which converts a homogeneous biochemical signal into an asymmetric response. Inspired by the leaf closure mechanism, we devise and test a mechanical metamaterial, which curls under homogeneous mechanical stimuli. This kind of metamaterial could find possible applications as a component in soft robotics and provides an example of bio-inspired design.

Drosera capensis | metamaterials | biomechanics | bending

The movements performed by carnivorous plants have excited interest and curiosity in scientists and laypeople for more than a century. Darwin was fascinated by these plants and reported in a seminal book (1) his 16-y-long observations, including a section on *Drosera capensis* L. (Droseraceae), a carnivorous plant with long leaves that fold around prey (*SI Appendix*, Figs. S1 and S2). In his studies, he tested an incredible number of different substances for their capacity to induce leaf closure and described the motion of the tentacles (1). Darwin noticed that this plant was excellently adapted for the special purpose of catching insects thanks to thin filaments and extremely adhesive secretions covering the leaves (2). Nowadays, we know that the adhesive and digestive secretions are produced by glandular hairs (i.e., the stalked hairs producing sticky mucillagine droplets on the tip) (3).

Most of the research activity on the leaf movement of carnivorous plants, including *D. capensis*, focuses on the underlying biochemical signaling. In particular, early studies (4, 5) show that the presence of a prey triggers a transfer of auxin, a plant growth hormone often involved in plant movement (6), from the tip of the leaf to the site of the capture. More recent papers also show the relevance of jasmonic acid, which is shown to trigger leaf closure, possibly working in combination with auxin (7), and they highlight the role of electrical signaling (8). The role played by mechanics has been mostly neglected in *D. capensis* leaf closure, despite its well-known importance in the motion of other carnivorous plants (9, 10), such as *Dionaea muscipula* J. Ellis snap trap (11) or the *Utricularia* suction trap (12). Those plants actuate their capture mechanisms by storing elastic energy that is then released through an extremely rapid buckling/unbuckling instability (11, 12). Similarly, a combination of turgor pressure and geometry was recently shown to be relevant for the explosive seed dispersal of *Cardamine hirsuta* (13). In contrast with those cases, the closure of *D. capensis* leaves occurs on much slower timescales, suggesting a different self-shaping mechanism (14–16).

Results

Macroscopic Leaf Closure Mechanics. We study the mechanism of leaf closure in *D. capensis* by performing a series of experimental recordings using milk drops of different volumes as prey and find that drops of volume of 10 μL or larger are able to induce complete closure (*SI Appendix*, Fig. S2 *A–F*). We place the milk drop at different locations along the leaf and record the leaf until it closes (Movies S1 and S2). The closure process can last as little as 20 min or extend up to 3 h depending on the plant conditions and the environment (*SI Appendix*, Fig. S2*G*). For instance, when the temperature is too high and the plant is under stress, the closure process occurs only partially (*SI Appendix*, Fig. S3). In some cases, we also observe intermittent behavior with lag phases where the closure process stops and then, resumes after.

To quantify the mechanical aspects of the closure process, we perform experiments by applying a counteracting force at the tip of a leaf until it is open as discussed in *SI Appendix* and

Significance

Understanding how carnivorous plants actuate leaf motion to capture their preys is an intriguing problem with potential applications for bio-inspired materials. Here, we show that bending of *Drosera capensis* leaves is programmed into its asymmetric cellular architecture and actuated by the action of growth hormones. A similar strategy can be exploited to design shape-changing metamaterials converting homogeneous stimuli into an asymmetric response.

Author contributions: C.A.M.L.P. and S.Z. designed research; C.A.M.L.P., M.C.L., S.B., S.M., C.F., D.R.-K., M.B., M.H., U.F., M.A., L.D.P., M.S., E.F., A.C., A.T., and A.V. performed research; M.C.L., S.B., S.M., L.D.P., Z.B., O.C., and S.Z. analyzed data; and C.A.M.L.P. and S.Z. wrote the paper.

The authors declare no conflict of interest.

This article is a PNAS Direct Submission.

[1]To whom correspondence may be addressed. Email: caterina.laporta@unimi.it or stefano.zapperi@unimi.it.

This article contains supporting information online at www.pnas.org/lookup/suppl/doi:10.1073/pnas.1904984116/-/DCSupplemental.

Published online August 26, 2019.

illustrated in Fig. 1 *A* and *B*. The force F needed to open the leaf is reported in Fig. 1*C* as a function of the distance l between the tip and the closure point. We can estimate theoretically this dependence assuming that the applied torque should balance the bending moment due to the curvature, which for a radius R, is given by $M = EI/((1-\nu^2)R)$, where E is the Young modulus of the leaf, ν is Poisson's ratio, and I is the second area moment given by $I = wh^3/12$ for a rectangular cross-section of thickness h and width w. We measure the leaf thickness and width, repeating the measurement over different leaves and different positions along the leaf, and find that $h = 0.46 \pm 0.1$ mm and $w = 4 \pm 1$ mm. The radius of curvature can be estimated from the images (Fig. 1*D*). In particular, we measure the radius of curvature R and the thickness h in a set of 6 closed leaves and then average the results. To estimate elastic parameters, we perform tensile tests on *D. capensis* leaves as discussed in *SI Appendix*. Loading curves display nonlinear stress–strain behavior, but a linear fit up to 20% strain yields an approximate Young modulus of $E = 4$ MPa (*SI Appendix*, Fig. S4). Using those values and $0.1 \leq \nu \leq 0.5$, we obtain a reasonable estimate for the force–length relation: for example, $F = EI/((1-\nu^2)Rl)$, where l is the distance between the tip and the closure point (lines in Fig. 1*C*). The results show that the precise value of Poisson's ratio ν has only a small effect.

To improve the theory, we perform more accurate finite element simulations (*SI Appendix* has details). A 2-dimensional geometry is taken from the outline of a typical plant leaf and then, extruded to create a 3-dimensional elastic structure of uniform thickness h. The structure is then allowed to relax from its initial configuration to a folded shape (*SI Appendix*, Fig. S5 and Movie S3) by prescribing a bending strain s matching the average value h/R measured experimentally in closed leaves (Fig. 1*D*). Next, the tip of the structure is displaced in order to open the leaf, holding a small surface region fixed and acting as pivot point (Fig. 1*E*). In these conditions, we find the reaction force at the tip of the leaf in the vertical direction and plot the result as a function of distance from leaf tip to pivot point (Fig. 1*B*), obtaining an excellent agreement with experimental measurements (Fig. 1*C*).

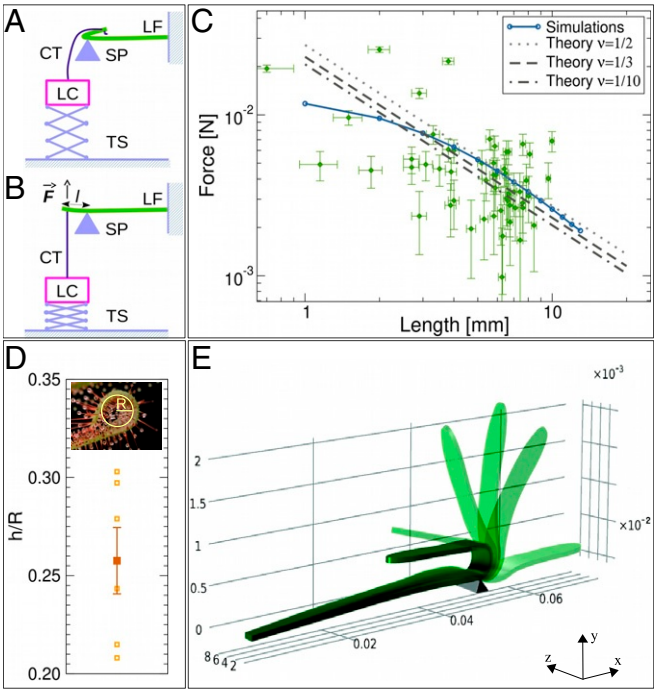

Fig. 1. Quantification of leaf (LF) closure forces. (*A*) Schematic of the experimental apparatus. In the closed trap, the support (SP) and the cotton thread (CT) do not exert any mechanical action on the LF. The load cell (LC) is zeroed. (*B*) In the open trap, the LC is lowered by using the translation stage (TS) until no curvature is apparent on the LF. The vertical force $\vec{F}$ exerted by the LF is balanced by the tension of the CT. (*C*) Measurement of the force needed to open a closed LF as a function of the distance between the tip and the location of the closure point. The black line is the result of finite element simulations (*E*), and the dashed lines are the results of the theory reported in the text using different values of Poisson's ratio. Error bars are due to measuring uncertainties. (*D*) The graph shows the ratio h/R between the thickness and the radius of curvature measured for 6 *D. capensis* closed leaves. Error bar is the SD. (*E*) LF conformations obtained from finite element simulations of the mechanical opening of the LF.

Asymmetric Structural Features Dictate Leaf Closure. In order to understand the microscopic determinants of leaf closure, we perform histological analysis of open and closed leaves sectioned along the longitudinal direction as illustrated in Fig. 2*A*. The leaves display a layered structure across the thickness, and we quantify the cell lengths ℓ along the elongated direction for cells in the upper and lower layers in open and closed leaves using image analysis (*SI Appendix*). The analysis shows that cells in the lower layer are considerably larger (almost double in length) than those in the upper layer for both closed ($\ell_{up} = 29 \pm 1$ μm, $\ell_{down} = 50 \pm 2$ μm) and open leaves ($\ell_{up} = 35 \pm 3$ μm, $\ell_{down} = 60 \pm 6$ μm). We performed a similar analysis sectioning the cell along the transverse direction (Fig. 2*B*) and did not detect any difference between cell lengths in the upper and lower layers (*SI Appendix* has details on the statistical analysis). To obtain a clearer representation cellular geometry and organization, we combine a sequence of 1-μm-thick transverse sections to obtain a 3-dimensional representation of the leaf structure. The result reported in Fig. 2*C* shows that cells display cylindrical shapes.

Since leaf closure was previously associated with growth hormones (4, 5), we investigate the presence of auxin (indole-3 acetic acid [IAA]) in closed and open leaves by immunofluorescence (*SI Appendix*, Fig. S6). As shown in Fig. 2*D*, closed leaves display almost 3 times larger expression of IAA with respect to open leaves (fold change $f_c = 2.8$ and $P = 10^{-5}$). In both closed and open leaves, however, a quantification of the signal intensity indicates no significant difference in IAA concentration for upper and lower layers ($f_c = 1.1$ and $P > 0.05$). Those results imply that leaf bending does not arise from differential expression of IAA along the leaf cross-section but is associated with a global increase of IAA concentration in the leaf. To confirm this point, we perform a gas chromatography–mass spectrometry (GCMS) assay (17). Auxin quantification by GCMS analyses is carried out in single-ion mode using 130 m/z as the target ion, whereas analyses separately acquired in full-scan mode are used to unequivocally identify the analyte. Each chromatographic peak was integrated, and the background was subtracted. The results show that the area under the peak corresponding to auxin is more than twice as large for closed leaves with respect to open leaves (the area ratio being $r_A = 2.8 \pm 0.6$ over $n = 3$ replicates) (*SI Appendix*, Fig. S7). The observed association between the increase of IAA and leaf bending does not prove, however, that a causal relationship exists. To address the issue, we immerse a leaf, still attached to the plant, into an IAA solution for 1 min and observe a subsequent upward bending (*SI Appendix*, Fig. S8). No bending is observed, however, when the leaf is immersed in a control medium.

The observation that leaf bending occurs in response to a global auxin increase suggests that leaf bending is programmed in the asymmetric cellular architecture. To investigate differential elongation across the leaf thickness, we detach leaves from the plant, cut them longitudinally, stain them with a fluorescent dye localizing on the cell walls (13), and immerse them for up

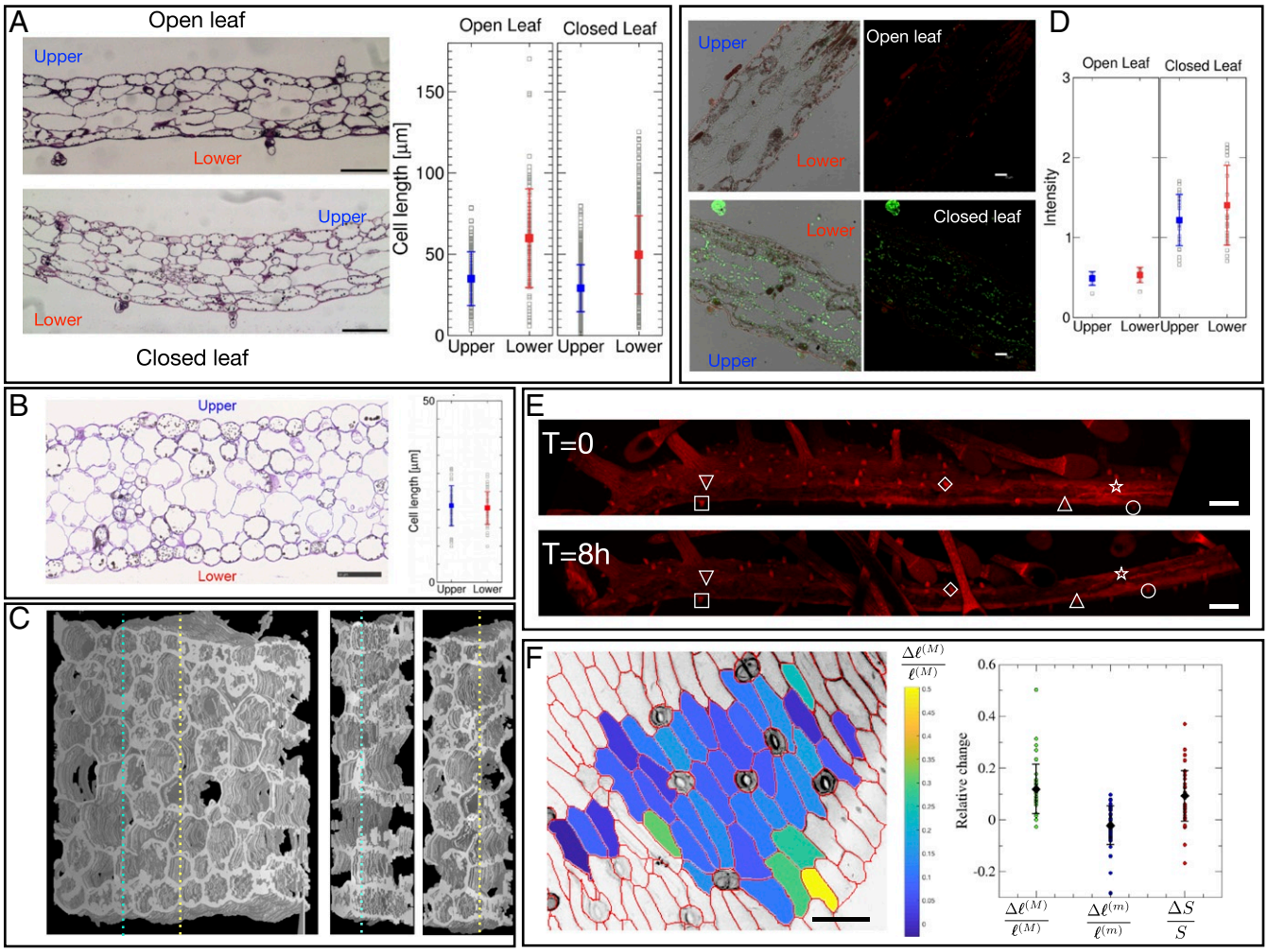

Fig. 2. Cellular architecture and growth induce leaf bending. (*A*) Longitudinal histological sections of *D. capensis* for open and closed leaves taken under 12.5× magnification. Cell lengths are reported together with average and SD. (Scale bar: 100 μm.) (*B*) Transverse histological section and associated cell lengths for an open leaf. (Scale bar: 50 μm.) (*C*) A 3-dimensional rendering of the leaf microstructure obtained by combining a set of transverse histological sections. Two sections of the same structure are also reported. (*D*) IAA distribution in open and closed leaves. IAA fluorescence intensity (green) increases considerably in closed leaves ($P = 10^{-5}$). Autofluorescent signal is reported in red. No difference in IAA intensity can be detected between upper and lower layers. Error bars are SDs. (Scale bar: 25 μm.) (*E*) Confocal images of leaves sectioned longitudinally before and after 8 h of treatment in a 10^{-7} M IAA solution. Markers can be used to determine the change in length in the upper and lower layers. (Scale bar: 200 μm.) (*F*) Confocal image of the bottom layer of a leaf. Cells are colored according to the relative elongation of the major axis after 20 h of treatment with a 10^{-7} M IAA solution. The graph reports the relative changes of the cells major and minor axes and areas. Details on the statistical analysis are reported in *SI Appendix*. (Scale bar: 50 μm.)

to 20 h in an IAA solution. In this condition, we observe considerable leaf bending (*SI Appendix*, Fig. S9) and record local cell deformations using a confocal microscope. Fig. 2*E* displays the same leaf section before and after exposure to the IAA solution. Using reference points on the surface, we can see that the lower layer elongates by around 12%, while the upper layer does not show any noticeable elongation. Hence, we focus on the lower surface and quantify the relative elongations of individual cells (*SI Appendix*). As shown in Fig. 2*F*, cells tend to elongate mostly along their major axis ($\Delta\ell^{(M)}/\ell^{(M)} = 0.12 \pm 0.01$), while the minor axis shrink slightly ($\Delta\ell^{(m)}/\ell^{(m)} = -0.02 \pm 0.01$), although the result is not statistically significant. As a result of this, cell areas tend to increase ($\Delta S/S = 0.02 \pm 0.01$).

To better understand the combined role of auxin increase and cellular architecture on leaf bending, we perform a finite element simulation using the cellular architecture extracted from Fig. 2*A*. In this simulation, we treat the cell walls and cell interiors as linear elastic materials with different mechanical properties (*SI Appendix* has details). To account for the presence of turgor pressure, we initialize the geometry such that the initial minimum energy configuration is a flat geometry where the cell walls are under tension and the cell interior is under compression. We simulate the effect of auxin by imposing cell wall loosening through a reduction in the Young's modulus of the cell wall material. The results of simulation shown in Fig. 3*A* (Movies S4 and S5) reveal a clear bending. We also observe an overall reduction in internal stresses as the structure bends (Fig. 3*B*). Moreover, we use the same finite element model to explore the contribution of turgor pressure in inducing leaf bending. We thus impose a homogeneous increase in the pressure of the cell interior without wall loosening. The result reported in Fig. 3*C* indicates that changes in turgor pressure would be able to induce bending even without auxin effects.

Notice that experimental observations show that, in closing *D. capensis* leaves, no bending occurs in the transverse direction (*SI Appendix*, Fig. S10), in agreement with a general property of thin sheets, where curvature along one principal direction suppresses curvature along the other (18). Hence, the 2-dimensional

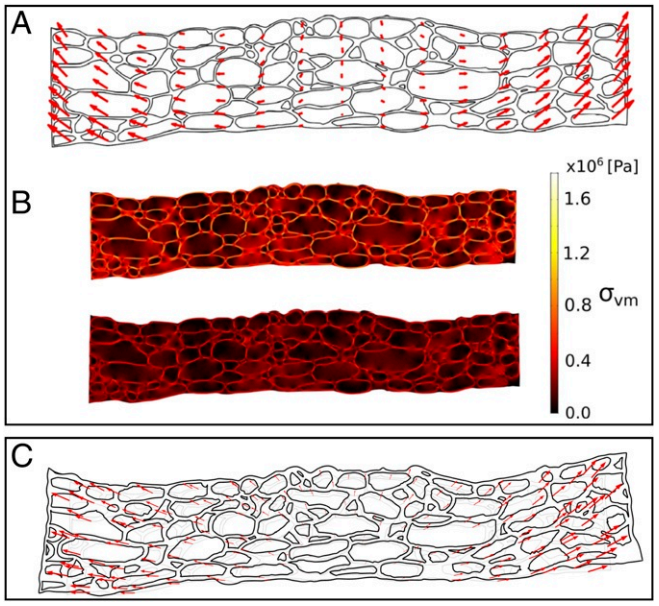

Fig. 3. Simulation of leaf bending due to structural asymmetry. (*A*) Finite element simulations of the evolution of the microstructure corresponding to Fig. 2*A*, where reducing the stiffness of cell walls leads to leaf bending. Arrows show the displacement of the structure as a result of wall loosening. (*B*) Von Mises stress distribution before (*Upper*) and after (*Lower*) cell wall loosening. (*C*) Bending induced by turgor pressure. Finite element method simulation of the response of the leaf structure to a global pressure increase in the cell interiors, which leads to bending.

geometry used in simulations should adequately represent the closure mechanism.

Mechanical Analogs of *D. capensis* Leaves. It is interesting to relate the self-shaping architectural design observed in *D. capensis* to other mechanical analogs working on similar principles. For instance, soft pneumatic bending actuators are often designed using an elastic tube with asymmetric surfaces realized by fiber reinforcement (19, 20) or coating (21). Surface asymmetries lead to bending in response to an increasing pressure.

We provide here another mechanical analog that highlights the role of geometry in programming the mechanical response. We devise a metamaterial that bends on uniaxial compression but does not rely on internal pressure. The design of the upper layer is based on the reentrant hexagonal lattice, which is known to have an auxetic behavior (22–25), while the lower lattice structure has the same geometry but with additional horizontal links (*SI Appendix*, Fig. S11). While auxetic behavior is not relevant for the *D. capensis* leaf, the example illustrates how to program an asymmetric response into the cellular structure. We perform finite element calculations of the uniaxial compression of the structure (*SI Appendix* has details). As the structure deforms under compression, the upper auxetic layer contracts, while the lower nonauxetic layer expands perpendicular to the long axis of the structure, resulting in a curvature being induced in the whole bilayer structure as shown in Fig. 4*A* (Movie S6). To confirm the result, we 3-dimensionally print the layered structure and perform a compression test (Fig. 4*B*). Experiments and simulations display similar results with respect to both the orthogonal bending and the mechanical characteristics (Fig. 4*C*). We also consider a control structure where both layers are formed by a regular nonauxetic lattice. Experiments and simulations show that, as expected, such a structure does not bend when compressed (*SI Appendix*, Fig. S12).

Using finite elements simulations, we can explore the response of the metamaterial to different stimuli. Fig. 4*D* reports simulations under 2 different types of loading: (*i*) uniform pressurization of the interior of the cells and (*ii*) a normal force applied to the top and bottom boundaries of the samples. Both of these loading conditions lead to bending and allow the structure to achieve angles that are much larger than those obtained under uniaxial compression with rigid boundaries as in Fig. 4*C*. Our metamaterial could be designed to capture objects as illustrated in Fig. 4*E*. Compression of the central region of the rod or pressurization of its cells leads to curling (Movie S7) reminiscent to the mechanism put in place by the *D. capensis* leaf to digest its prey. The carnivorous plant uses biochemical signaling to trigger the motion, while in the metamaterial, all action is purely mechanical.

Discussion

In summary, we investigated the bending of *D. capensis* leaves, performing direct measurement of the forces involved in leaf closure and their relationship with microstructural features and biochemical signals. Our results show that, in contrast to other well-studied examples of plant movement as in gravitotropism (26) or phototropism (27), where bending is due to differential growth owing to asymmetric auxin distribution, in *D. capensis*, auxin is distributed homogeneously across the leaf, while the microstructure is asymmetric. Hence, bending is encoded in the cellular architecture of leaf that is able to convert an isotropic biochemical signal into an asymmetric response. Using structural asymmetries to induce bending is also observed in other plants, notably in the opening of chiral seed pods (14). We can find further intriguing analogies with animals endowed with a hydrostatic skeleton, such as earthworms, that bend their body, combining local stiffening and internal fluid pressure redistribution (28).

While motion in response to stimuli is intrinsic to the natural world, incorporating prescribed, reversible motion into engineering materials and structures remains an open problem with great potential (29). As such, the mechanism underlying the

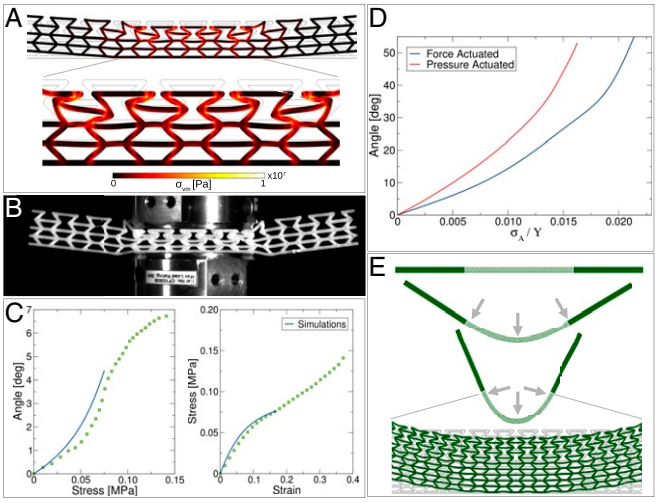

Fig. 4. Metamaterial designed to bend reversibly under homogeneous stimuli. (*A*) Finite element simulations of the bending of a metamaterial rod under orthogonal compression. The color is associated with Von Mises stress. *Lower* is a magnification of *Upper*. (*B*) Orthogonal compression of the 3-dimensional printed rod displays reversible bending. (*C*) Stress dependence of the bending angle and the stress–strain curves are correctly reproduced by finite element simulations. Points show experimental data, and lines show results of simulation. (*D*) Stress dependence of the bending angle for the model with 2 different loading conditions as reported in the text. (*E*) Snapshots of a finite element simulation of a structure based on the metamaterial, curling around the point of application.

movements in carnivorous plants could provide inspiration for the design of bio-inspired materials with advanced functionalities (30–32). In this paper, we illustrate this point by designing a metamaterial structure that responds asymmetrically to a symmetric mechanical stimulus. One can envisage several possible applications based on metamaterials, as in the example provided here, or more generally, on bilayers with heterogeneous structures. Examples include mechanical actuators (33, 34) or sensors (35), with possible uses in soft robotics (36), smart surfaces (37, 38), drone aircraft wing morphing (39), and reconfigurable materials (40). The general advantage of soft robotic components compared with usual rigid components is the extreme flexibility that is essential to deal with dynamic and uncertain tasks and provide safe physical contacts with delicate materials, such as living matter (41). Purely mechanical actuators do not rely on electronics and electricity and could thus be useful for applications designed to operate in harsh environments, including under the sea where electricity is hard to manage or in strong radiation environments, such as nuclear power plants.

Materials and Methods

Plant Material and Culture Conditions. Experimental plants were grown in a tropical greenhouse; subadult or adult plants (3 mo old) of similar size were used for all of the experiments.

Time Lapse of Leaf Closure of *D. capensis* in Response to Different External Stimuli. Drops of 10 μL of cow milk are applied on the leaf in different positions, and the images are immediately acquired using the color camera with a time lapse of 1 min. A similar procedure is applied after immersing the leaves in a 2-mL solution containing IAA 10^{-7} M or 0.001% ethanol in bidistilled water for 60 s at room temperature (RT).

Histological Analysis. Small pieces (thickness: 0.5 mm; length: 3 to 4 mm) of both open and closed leaves were immediately processed following standard procedures and embedded in pure resin. Longitudinal and transverse semithin sections (1 μm) were obtained, stained with crystal violet and basic fuchsin, and then, observed under a light microscope. To obtain a 3-dimensional rendering of the structure, images are first globally translated, rotated, and sheared to correct for the lack of alignment between successive cuts.

Cell Wall Staining and Confocal Imaging. To visualize elongation of cells during the closure in sectioned leaves, the traps were incubated in 1 mL of 0.1% propidium iodide for 10 min at RT immediately after being cut in the longitudinal direction and imaged with a confocal microscope before and after exposing them to an IAA solution.

Quantification of Cell Lengths. The quantification of the cell lengths from histological sections was performed using the Image Processing Toolbox of Matlab.

Immunofluorescence Assay. Small pieces of both open and closed leaves were immediately incubated in 4% 1-Ethyl-3-(3-dimethylaminopropyl) carbodiimide/phosphate-buffered saline (PBS), fixed in 4% paraformaldehyde/PBS, and dehydrated at RT. After an overnight at 60 °C in xylene/paraffin, the samples were maintained in 100% paraffin for 8 h. Then, sections were collected, dewaxed, rehydrated, and washed, and slides were incubated in 10% dimethyl sulfoxide and 3% Nonidet P-40 in 10 mM PBS for 30 min at RT and then, in blocking solution for 45 min at RT. After washing in PBS, the slides were incubated with anti-IAA antibody (1:600; Agrisera AS06 193) in blocking solution overnight at 4 °C and finally, with goat anti-rabbit antibody (1:250; ab150077; Abcam) for 45 min at RT. Image stacks were obtained in a confocal microscope, and the resulting intensity was quantified. More details are found in *SI Appendix*.

Auxin Quantification in Leaves by GCMS. Auxin was quantified using GCMS according to ref. 17. More details are in *SI Appendix*.

Tensile Tests. Uniaxial tensile tests were carried out by a dynamical mechanical thermal analyzer. Leaf specimens were vertically clamped, and tensile measurements were performed in force controlled mode with a loading rate of 1 N/min up to sample fracture at a stabilized temperature of 30 °C.

Measurement of the Bending Moment. Bending moment was measured using the load cell illustrated in Fig. 1 *A* and *B* and is fully described in *SI Appendix*.

Three-dimensional Printing. Three-dimensional models of the simulated structures have been produced by adding width to each bond. Samples are then produced by means of 3-dimensional printing using the fused deposition modeling technique.

Compression Tests. Printed metamaterial samples with $x \times y \times z$ dimensions of $14 \times 1.5 \times 1$ cm were put under compression load applied by a testing machine, which applied a constant strain rate of 0.02 mm/s up to 1-kN force limitation.

Finite Element Calculations. All finite element simulations were performed in COMSOL Multiphysics 5.3 using the solid mechanics module. In all cases, linear stress–strain relationships were assumed for the constituent material, and mesh refinement studies were undertaken to ensure convergence of results.

Statistical Analysis. Statistical analysis for the data reported in Fig. 2 was performed using the Kolmogorov–Smirnov test.

ACKNOWLEDGMENTS. S.M., Z.B., and S.Z. are supported by European Research Council (ERC) Advanced Grant SIZEFFECTS. S.Z. acknowledges support from ERC Proof of Concept Grant METADESIGN and Academy of Finland FiDiPro Program Project 13282993. M.H. is supported by Academy of Finland Project 251748 (Center of Excellence Program 2012 to 2017). D.R.-K. acknowledges funding support from the Academy of Finland postdoctoral grant program. A.V. acknowledges partial support from the "Greenmechanics" Project of the University of Milan. We thank M. Caccianiga, F. Di Renzo, M. R. Fumagalli, A. Moscatelli, and E. Onelli for useful discussions; V Parravicini for his contribution to the cultivation of the plants; and F. Font-Clos and R. Guerra for critical reading of the manuscript.

1. C. Darwin, *Insectivorous Plants* (John Murray, London, 1875).
2. W. Adlassnig, T. Lendl, M. Peroutka, I. Lang, "Deadly glue—adhesive traps of carnivorous plants" in *Biological Adhesive Systems*, J. von Byern, I. Grunwald, Eds. (Springer, 2010), pp. 15–28.
3. Y. Naidoo, S. Heneidak, Morphological investigation of glandular hairs on drosera capensis leaves with an ultrastructural study of the sessile glands. *Botany* **91**, 234–241 (2013).
4. M. Bopp, I. Weber, Hormonal regulation of the leaf blade movement of drosera capensis. *Physiol. Plant.* **53**, 491–496 (1981).
5. M. Bopp, E. Weiler, Leaf blade movement of drosera and auxin distribution. *Naturwissenschaften* **72**, 434 (1985).
6. A. Santner, L. I. Calderon-Villalobos, M. Estelle, Plant hormones are versatile chemical regulators of plant growth. *Nat. Chem. Biol.* **5**, 301–307 (2009).
7. Y. Nakamura, M. Reichelt, V. E. Mayer, A. Mithöfer, Jasmonates trigger prey-induced formation of 'outer stomach' in carnivorous sundew plants. *Proc. Biol. Sci.* **280**, 20130228 (2013).
8. M. Krausko *et al.*, The role of electrical and jasmonate signalling in the recognition of captured prey in the carnivorous sundew plant drosera capensis. *New Phytol.* **213**, 1818–1835 (2017).
9. J. M. Skotheim, L. Mahadevan, Physical limits and design principles for plant and fungal movements. *Science* **308**, 1308–1310 (2005).
10. H. Liang, L. Mahadevan, The shape of a long leaf. *Proc. Natl. Acad. Sci. U.S.A.* **106**, 22049–22054 (2009).
11. Y. Forterre, J. M. Skotheim, J. Dumais, L. Mahadevan, How the venus flytrap snaps. *Nature* **433**, 421–425 (2005).
12. O. Vincent *et al.*, Ultra-fast underwater suction traps. *Proc. Biol. Sci.* **278**, 2909–2914 (2011).
13. H. Hofhuis *et al.*, Morphomechanical innovation drives explosive seed dispersal. *Cell* **166**, 222–233 (2016).
14. S. Armon, E. Efrati, R. Kupferman, E. Sharon, Geometry and mechanics in the opening of chiral seed pods. *Science* **333**, 1726–1730 (2011).
15. I. Burgert, P. Fratzl, Actuation systems in plants as prototypes for bioinspired devices. *Philos. Trans. A Math. Phys. Eng. Sci.* **367**, 1541–1557 (2009).
16. S. Li, K. W. Wang, Plant-inspired adaptive structures and materials for morphing and actuation: A review. *Bioinspir. Biomim.* **12**, 011001 (2016).
17. L. S. Barkawi, Y. Y. Tam, J. A. Tillman, J. Normanly, J. D. Cohen, A high-throughput method for the quantitative analysis of auxins. *Nat. Protoc.* **5**, 1609–1618 (2010).
18. V. Pini *et al.*, How two-dimensional bending can extraordinarily stiffen thin sheets. *Sci. Rep.* **6**, 29627 (2016).
19. K. Suzumori, S. Endo, T. Kanda, N. Kato, H. Suzuki, "A bending pneumatic rubber actuator realizing soft-bodied manta swimming robot" in *Proceedings of the 2007 IEEE International Conference on Robotics and Automation* (IEEE, Piscataway, NJ, 2007), pp. 4975–4980.

20. P. Polygerinos *et al.*, Modeling of soft fiber-reinforced bending actuators. *IEEE Trans. Robot.* **31**, 778–789 (2015).
21. Y. Sun, Y. S. Song, J. Paik, "Characterization of silicone rubber based soft pneumatic actuators" in *Proceedings of the 2013 IEEE/RSJ International Conference on Intelligent Robots and Systems* (IEEE, Piscataway, NJ, 2013), pp. 4446–4453.
22. R. Lakes, Foam structures with a negative Poisson's ratio. *Science* **235**, 1038–1040 (1987).
23. L. J. Gibson, M. F. Ashby, G. S. Schajer, C. I. Robertson, The mechanics of two-dimensional cellular materials. *Proc. R. Soc. Lond.* **382**, 25–42 (1982).
24. K. E. Evans, A. Alderson, F. R. Christian, Auxetic two-dimensional polymer networks. An example of tailoring geometry for specific mechanical properties. *J. Chem. Soc. Faraday Trans.* **91**, 2671 (1995).
25. B. Xu *et al.*, Making negative Poisson's ratio microstructures by soft lithography. *Adv. Mater.* **11**, 1186–1189 (1999).
26. I. Ottenschläger *et al.*, Gravity-regulated differential auxin transport from columella to lateral root cap cells. *Proc. Natl. Acad. Sci. U.S.A.* **100**, 2987–2991 (2003).
27. J. Friml, J. Wiśniewska, E. Benková, K. Mendgen, K. Palme, Lateral relocation of auxin efflux regulator pin3 mediates tropism in arabidopsis. *Nature* **415**, 806–809 (2002).
28. W. M. Kier, The diversity of hydrostatic skeletons. *J. Exp. Biol.* **215**, 1247–1257 (2012).
29. A. Sidorenko, T. Krupenkin, A. Taylor, P. Fratzl, J. Aizenberg, Reversible switching of hydrogel-actuated nanostructures into complex micropatterns. *Science* **315** 487–490 (2007).
30. P. Fratzl, Biomimetic materials research: What can we really learn from nature's structural materials? *J. R. Soc. Interface* **4**, 637–642 (2007).
31. P. Fratzl, F. G. Barth, Biomaterial systems for mechanosensing and actuation. *Nature* **462** 442–448 (2009).
32. A. R. Studart, Biologically inspired dynamic material systems. *Angew. Chem. Int. Ed. Engl.* **54**, 3400–3416 (2015).
33. J. T. B. Overvelde, T. Kloek, J. J. A. D'haen, K. Bertoldi, Amplifying the response of soft actuators by harnessing snap-through instabilities. *Proc. Natl. Acad. Sci. U.S.A.* **112**, 10863–10868 (2015).
34. F. Connolly, C. J. Walsh, K. Bertoldi, Automatic design of fiber-reinforced soft actuators for trajectory matching. *Proc. Natl. Acad. Sci. U.S.A.* **114**, 51–56 (2017).
35. S. Babaee *et al.*, 3D soft metamaterials with negative Poisson's ratio. *Adv. Mater.* **25**, 5044–5049 (2013).
36. D. Rus, M. T. Tolley, Design, fabrication and control of soft robots. *Nature* **521**, 467–475 (2015).
37. M. A. Dias, J. A. Hanna, C. D. Santangelo, Programmed buckling by controlled lateral swelling in a thin elastic sheet. *Phys. Rev. E* **84**, 036603 (2011).
38. A. Lamoureux, K. Lee, M. Shlian, S. R. Forrest, M. Shtein, Dynamic kirigami structures for integrated solar tracking. *Nat. Commun.* **6**, 8092 (2015).
39. M. Di Luca, S. Mintchev, G. Heitz, F. Noca, D. Floreano, Bioinspired morphing wings for extended flight envelope and roll control of small drones. *Interface Focus* **7**, 20160092 (2017).
40. J. T. B. Overvelde, J. C. Weaver, C. Hoberman, K. Bertoldi, Rational design of reconfigurable prismatic architected materials. *Nature* **541**, 347–352 (2017).
41. N. G. Cheng, A. Gopinath, L. Wang, K. Iagnemma, A. E. Hosoi, Thermally tunable, self-healing composites for soft robotic applications. *Macromol. Mater. Eng.* **299**, 1279–1284 (2014).